Rapid appearance and local toxicity of amyloid-beta plaques in a mouse model of Alzheimer's disease

Published In:
Nature

Rapid appearance and local toxicity of amyloid-β plaques in a mouse model of Alzheimer's disease

Melanie Meyer-Luehmann[1], **Tara L. Spires-Jones**[1], **Claudia Prada**[1], **Monica Garcia-Alloza**[1], **Alix de Calignon**[1], **Anete Rozkalne**[1], **Jessica Koenigsknecht-Talboo**[2], **David M. Holtzman**[2], **Brian J. Bacskai**[1], and **Bradley T. Hyman**[1]

[1]Alzheimer's Disease Research Laboratory, Department of Neurology, MassGeneral Institute for Neurodegenerative Disease, Massachusetts General Hospital, Harvard Medical School, Charlestown, Massachusetts 02129, USA.

[2]Department of Neurology, Washington University School of Medicine, St Louis, Missouri 63110, USA.

Abstract

Senile plaques accumulate over the course of decades in the brains of patients with Alzheimer's disease. A fundamental tenet of the amyloid hypothesis of Alzheimer's disease is that the deposition of amyloid-β precedes and induces the neuronal abnormalities that underlie dementia[1]. This idea has been challenged, however, by the suggestion that alterations in axonal trafficking and morphological abnormalities precede and lead to senile plaques[2]. The role of microglia in accelerating or retarding these processes has been uncertain. To investigate the temporal relation between plaque formation and the changes in local neuritic architecture, we used longitudinal *in vivo* multiphoton microscopy to sequentially image young APPswe/PS1d9xYFP (B6C3-YFP) transgenic mice[3]. Here we show that plaques form extraordinarily quickly, over 24 h. Within 1–2 days of a new plaque's appearance, microglia are activated and recruited to the site. Progressive neuritic changes ensue, leading to increasingly dysmorphic neurites over the next days to weeks. These data establish plaques as a critical mediator of neuritic pathology.

To explore the formation of amyloid plaques and to determine the effects of newly formed dense-cored plaques on the microarchitecture of the brain, we have developed a novel *in vivo* multiphoton imaging technique. This recognizes newly formed plaques and allows monitoring of their immediate vicinity thereafter to determine the rate of their formation and the temporal sequence of pathophysiological events. We imaged young (5- to 6-month-old) B6C3-YFP mice, an age when plaques begin to appear[4] (Fig. 1). We used three-colour imaging to establish fiduciary markers for repeated imaging: YFP positive neurons, dendrites and axons in the cortex, methoxy-XO4-labelled fibrillar amyloid-β deposits in the parenchyma and on vessel walls, and a fluorescent angiogram with Texas red dextran to image blood vessels. A volume of cortex (lamina I–III) that initially did not contain plaques was re-imaged until repeat imaging detected a new plaque, establishing its 'birthday'. To ensure that the appearance of a new plaque did not simply reflect a greater depth of imaging or a slightly different imaging volume, we went through each image stack and compared

them with previous sessions. New plaques were accepted only if a uniquely identifiable fiduciary point, such as a blood vessel or a dendritic process, could be unambiguously noted in a deeper imaging plane.

We postulated that we would occasionally observe the appearance and growth of new plaques within an imaging volume if the time interval between imaging sessions was long enough. From one weekly imaging session to the next, most of the sites remained unchanged (Supplementary Fig. 1a–c). However, we identified 14 new plaques: instances in which a plaque appeared in a second imaging session in a volume that had clearly been unoccupied in the first images one week earlier (Fig. 1a–c).

We examined the spatial relation between newly identified plaques and blood vessels. Measurements of the distance between vessel wall and the edge of a plaque confirmed that dense-core plaques develop close to but not within blood vessels (9.1 ± 3.9 µm from blood vessels). As a control, 70 randomly placed, plaque-sized objects had an average distance of 8.4±11.2 µm from a vessel. New plaques therefore do not form any closer to vessels than would be expected by chance, in accord with an earlier study of human Alzheimer's disease [5]. Furthermore, multiphoton microscopic images showed that newly formed plaques were not penetrated by blood vessels[6], suggesting only a limited direct role of blood vessels in the formation of dense-core plaques.

To examine whether the phenotype of plaque formation in as short a period as one week was unique to the aggressive APP/PS1 transgenic mouse model, we used a mouse line that has a slower progression of disease (Tg2576)[7]. Seven Tg2576 transgenic mice (11 months) were imaged weekly, and fourteen additional new plaques were observed, suggesting that the rapid plaque formation is not restricted to one mouse model (Supplementary Fig. 2).

We next imaged the B6C3-YFP mice on a daily basis for up to six days in a row and/or on a weekly basis for up to three weeks (Fig. 1d–i). To our surprise, senile plaque formation is a very rapid event, with five new plaques appearing precipitously within 24 h after the last imaging session. However, plaque formation is a rare event. Combining our experiments of daily and weekly imaging, a total of 26 new plaques were found in 14 animals over 238 sites, imaged a total of 1,285 times.

These newly formed plaques were then re-imaged over days to weeks to determine their growth pattern. Measurements of plaque area over several imaging sessions revealed that they do not change in size after about the first 24 h, regardless of whether they had small or large diameters when they were first imaged (Fig. 1j). To examine whether imaging procedures had affected the observed plaque characteristics, we compared *in vivo* measures with those obtained from post-mortem analysis of mice either after our imaging protocols or with naive mice that had never been imaged. These analyses confirmed that the newly formed plaques are not significantly different in area or diameter from those observed post mortem and therefore represent typical plaques (Supplementary Fig. 3). Furthermore, the size distribution of new plaques compares well with that of all plaques seen post mortem in non-imaged mice (Supplementary Fig. 3). The shape of this histogram is also quite similar to that observed in analyses of human patients with Alzheimer's disease[8].

Several studies have shown that microglia surround senile plaques both in patients with Alzheimer's disease and transgenic mouse models [9,10] although their role remains elusive[11,12]. It has been proposed that activated microglia clear amyloid deposits[13], are the nidus for initiation of amyloid fibrils[14] or restrict plaques[15]. To study the interaction between newly formed amyloid plaques and microglia, we imaged microglia before and after plaque formation (Fig. 2) in PDAPP mice crossed with a line that expresses enhanced green fluorescent protein (EGFP) in microglia[16,17]. In this third APP transgenic line, we

again found rapid formation of new plaques, with seven new plaques occurring within 24 h. Microglia were attracted to the site of plaque formation within a day (Fig. 2b). None of the new plaques occurred immediately adjacent to resident microglia, suggesting that microglia do not form the nidus of new plaques. We did not observe any plaques being cleared by this microglial response. This suggests that, unless further activated[18], microglia do not successfully clear plaques but instead may well restrict their growth, leading to the observed steady state of plaque size after initial formation.

Stokin *et al.* recently proposed that amyloid deposits followed axonal trafficking defects, marked morphologically as neuritic dystrophies. In contrast, amyloid deposition has been postulated to cause neuronal alterations[1,19]. To study the temporal relation between newly formed plaques and dystrophic neurites, we compared the shape and trajectories of yellow fluorescent protein (YFP) fluorescent neurites before and after plaque formation in B6C3-YFP animals (Fig. 3). These neurites were morphologically normal in the volume of cortex one day before plaque formation. By contrast, in the days after plaque formation, progressive neuritic alterations were evident: from a smooth bend around the new plaque to very tortuous changes identical in appearance to dystrophic neurites seen in Alzheimer's disease[20]. The degree of neuritic deformation is best illustrated in individual image slices (Fig. 3a, c) as well as in three-dimensional reconstructions (Fig. 3b, d).

Neurite curvature was quantitatively analysed[20,21] from the *in vivo* images around each new plaque ($n = 12$) as well as more than 50 µm away from it, and compared with equivalent measures in randomly selected fields from YFP control mice. As expected, neurites were essentially straight, and unchanged in morphology over several weeks of imaging in YFP mice. In the B6C3-YFP mice, in the immediate vicinity of plaques the tortuosity increased gradually over the first week (Fig. 3e, $P < 0.0001$). Post-mortem analysis of neuritic curvature ($n = 218$) taken of randomly selected plaques observed at the time of death confirmed that neuritic curvature measured around new plaques one week after their formation is indistinguishable from the same measurements taken around all plaques (1.048 ± 0.02 versus 1.052 ± 0.014). This suggests that neuritic changes occur rapidly and to essentially a maximal extent over the first week of a plaque's presence.

We next analysed changes in neurites near plaques on a daily basis. No change from baseline in neuritic curvature was detected on the day of plaque appearance (Fig. 3f). Neuritic alterations were first evident one day after the occurrence of a new plaque, indicating that neuritic deformation is a secondary effect of plaque development ($n = 15$; analysis of variance (ANOVA $P = 0.02$)). After two days the damage became more prominent; after five days it resembled the more robust neuritic damage seen after one week (Fig. 3e, f). Thus the neurite changes progressed over days after a short lag phase (although the imaging would not detect more subtle changes in cytoskeleton that might occur even earlier). In several instances, frank neuritic dystrophies appeared on a previously normal dendrite three to four days after the first appearance of a new senile plaque (Fig. 1). In almost all instances of new plaque formation (11 of 13 new plaques in which concurrent observation of YFP filled neurites was obtained), frank neuritic dystrophies followed plaque formation within one week (Supplementary Fig. 4a, b) (χ^2 test $P < 0.001$). Post-mortem immunostaining suggested that both dendritic and axonal elements contribute to these dystrophic neurites (Supplementary Fig. 5).

Axonal dystrophies can be observed both near plaques and in the neuropil without a plaque. Such dystrophies have been hypothesized to anticipate the location of plaques[2]. We tested the idea that areas with a high density of dystrophies would be a prime location for plaque development. We tracked sites containing dystrophies but no plaques over days to weeks, but never observed a new plaque appearing at a site of high dystrophic neurite density.

Instead, it seemed that these dystrophic processes are quite dynamic. Out of ten examples, 40% of the dystrophic neurites changed morphologies (with some even resolving completely) and only 60% were unaltered over one to two weeks of imaging (Supplementary Fig. 4c–f).

Because our *in vivo* amyloid imaging agent, methoxy-XO4, would not report amyloid-β deposits that do not contain β-pleated sheets, we compared immunostaining for amyloid-β and methoxy-XO4 in histologic specimens to look for diffuse plaques in 8-month-old B6C3-YFP mice. All of the plaques were dense-core in morphology, with co-staining of amyloid-β immunofluorescence and methoxy-XO4 (Supplementary Fig. 6). Because these mice develop innumerable plaques, the absence of any plaques with a diffuse morphology argues against the idea that dense-core plaques represent a remodelled form of diffuse, 'primitive' plaques.

Longitudinal *in vivo* imaging of plaque formation provides a new appreciation for the kinetics of the amyloid deposition process *in vivo*, and demonstrates the temporal relations between amyloid deposits, microglial recruitment and activation, and neuritic changes. Although it takes months for many plaques to accumulate, even in accelerated mouse models of Alzheimer's disease[7,16], our data show that an individual dense-core plaque's formation unexpectedly represents an acute event. These results are surprising because it has been generally accepted, based on *in vitro* studies of protein aggregation, that amyloid-β aggregation is time dependent and follows a relatively slow nucleation-dependent polymerization process[22]. It is possible that submicroscopic nuclei may be present in the cortex[23], perhaps related to the recently reported amyloid-β oligomeric forms[24,25], as precursors to this sudden growth.

Observing the 'birthday' of new plaques provides the opportunity to examine directly whether dystrophic neurites near amyloid deposits precede or follow amyloid deposition. Our data strongly argue in favour of the latter, and suggest a period of several days after plaque formation during which progressive cytoskeletal derangements occur in neurites near a plaque. The observation of a local microenvironment in which microglia are recruited and activated after plaque formation further supports a model in which plaques act as a reservoir of bioactive molecules (Supplementary Fig. 7), which subsequently lead to neuronal alterations[19] including local loss of dendritic spines and axonal dystrophies[26]. These data thus lead to a model consistent with a prediction of the amyloid hypothesis in which amyloid deposition, activation and recruitment of microglia and local neuritic changes play out as a sequential cascade leading to neurodegeneration[1].

The current observations provide narrow parameters on the kinetics of plaque growth and stabilization through microglia, and raise the possibility that the years-long degenerative process of Alzheimer's disease is marked by innumerable sudden changes in cortical structure. Altering the kinetics of this process may well change the rate of progression of Alzheimer's disease.

METHODS SUMMARY

Three different APP transgenic mouse lines were used in this study (B6C3-YFP, Tg2576 and PDAPP$^{+/-}$xCX3CR1-GFP$^{+/-}$). Cranial window surgery was performed followed by either daily or weekly *in vivo* multiphoton microscopy[26]. After completion of *in vivo* imaging, frozen brain sections were stained immunohistochemically. Image analysis measuring plaque size or neuritic curvature was done using Image J (National Institutes of Health freeware).

Full Methods and any associated references are available in the online version of the paper at www.nature.com/nature.

METHODS

Animals and surgical procedures

APPswe/PS1d9xYFP (B6C3-YFP; obtained from Jackson Laboratory, Bar Harbor, Maine) and Tg2576[7] transgenic mice were used in this study; YFP transgenic mice served as controls (a total of six double transgenic, five transgenic and four littermate controls expressing only the YFP transgene were followed through three to eight weekly and one to six daily imaging sessions)[4]. B6C3-YFP mice overexpress YFP in a subset of cortical neurons, and start to develop plaques in the neocortex between five and seven months of age. In addition, homozygous PDAPP mice[16] were crossed with homozygous CX3CR1-GFP mice[17], and two female PDAPP^{+/−}×CX3CR1-GFP^{+/−} transgenic mice at the age of 18 months were used in this study and imaged for three consecutive days. All animal work conformed to National Institutes of Health and institutional guidelines. Cranial window surgery was done under isoflurane anaesthesia by installing a glass window 6 mm in diameter on top of the brain. One day before surgical procedure, mice received an intraperitoneal injection of methoxy-XO4 (5 mg kg^{-1}), a fluorescent compound that crosses the blood–brain barrier and binds to amyloid plaques[27].

Multiphoton imaging

In vivo imaging of amyloid pathology, YFP-positive neuronal processes and blood vessels in the living mouse brain was performed on a Bio-Rad 1024ES multiphoton microscope (Bio-Rad Laboratories), mounted on an Olympus BX50WI upright microscope (Olympus Optical). Texas red dextran (molecular mass 70,000 daltons, 12.5 mg/ml in sterile phosphate-buffered saline (Molecular Probes)) was injected into the lateral tail vein and served as a guide to repeatedly find the same sites in the brain by providing a fluorescent angiogram. A wax ring was placed around the coverslip of the cortical window and filled with distilled water to create a well for an Olympus 20X dipping objective (numerical aperture 0.95). A mode-locked Ti:Sapphire laser (MaiTai, Spectra-Physics) generated two-photon fluorescence with 800 nm excitation, and detectors containing three photomultiplier tubes (Hamamatsu Photonics) collected emitted light in the range of 380–480, 500–540 and 560–650 nm. During each imaging session, images at low resolution (615 µm × 615 µm × 5 µm sections; 10–20 sections per stack) were captured to provide an overview of the area, followed by images with high resolution (approximately 150 µm × 150 µm × 1 µm sections; 15–50 sections per stack) to zoom in on a specific area. Observations of the same neurites and plaques over time were made using the four-dimensional stack acquisition feature within imaging sessions and by taking images of the same neurites and plaques in subsequent weekly imaging sessions.

At the end of imaging sessions, mice were allowed to recover on a heating pad and placed singly in their home cage. For subsequent weekly or daily imaging sessions, mice were again injected with methoxy-XO4 the day before imaging, then anaesthetized, injected with Texas red dextran intravenously, and observed under the multi-photon microscope as described above. After the last imaging session, mice were euthanized with an overdose of avertin (400 mg kg^{-1}) and the brains immersion-fixed in 4% paraformaldehyde in phosphate buffer with 15% glycerol cryoprotectant.

Image processing and data analysis

To exclude motion artefacts induced by heartbeat and breathing, image stacks were aligned using AutoDeblur software (AutoQuant). Two-dimensional projections of stacks from each

of the three channels were combined in Adobe Photoshop 7 (Adobe Systems). Reconstructions of neurites, plaques and amyloid angiopathy in three dimensions were performed by reconstructing software from synapse web at the Medical College of Georgia (www.synapses.mcg.edu).

Plaque size (area in square micrometres) of the new plaques was assessed along with the distance from each plaque edge to the nearest blood vessel. In images from non-transgenic control animals, acquired with fluorescent angiograms, simulations were performed by randomly placing two phantom plaques with the average new plaques to measure the distances of the plaque edge to the nearest blood vessels. The coordinates of the phantom plaques were determined by generating random numbers from 0 to 512. Data were expressed as mean±standard deviation from the mean.

Quantitative measurements were performed in Image J (National Institutes of Health freeware). The distance of neurites from the nearest plaque (if present) was determined as the average of the distance measured from each end and the midpoint of the neurite segment to the edge of the plaque. Neurite curvature ratios were calculated by dividing the total length of a neurite by the end-to-end distance of a neurite segment[20,26]. Dystrophic neurites with swellings greater than 2.5 µm were classified as dystrophic and included in the study. Data were expressed as mean ± standard deviation from the mean. Group means were compared by ANOVA in the StatView program (SAS Institute, Inc.). The level of significance was set at $P \leq 0.05$.

Immunohistochemistry

The brains were frozen and serial coronal sections 25 µm thick were cut on a freezing sliding microtome. Sections were immunostained with the monoclonal primary antibodies 3D6 (Elan Pharmaceuticals), Smi312 (Covance Research Products, Inc.), Smi32 (Sternberger Monoclonals), synaptophysin (Abcam) followed by secondary anti-mouse conjugated cyanine 3 (Cy3) (Jackson ImmunoResearch). Additionally, three brains of 8-month-old B6C3 mice were cut in coronal sections 45 µm thick and stained post mortem with methoxy-XO4. Images were acquired either with an upright Olympus Optical BX51 fluorescence microscope with an Olympus Optical DP70 camera or with a Zeiss LSM510 Meta confocal microscope and analysed using Image J (National Institutes of Health freeware) and Adobe Photoshop 7 (Adobe Systems). The mean area of plaque size post mortem was determined by using Bioquant image analysis software.

Supplementary Material

Refer to Web version on PubMed Central for supplementary material.

Acknowledgments

References

1. Hardy J, Selkoe DJ. The amyloid hypothesis of Alzheimer's disease: progress and problems on the road to therapeutics. Science. 2002; 297:353–356. [PubMed: 12130773]

2. Stokin GB, et al. Axonopathy and transport deficits early in the pathogenesis of Alzheimer's disease. Science. 2005; 307:1282–1288. [PubMed: 15731448]

3. Jankowsky JL, et al. Co-expression of multiple transgenes in mouse CNS: a comparison of strategies. Biomol. Eng. 2001; 17:157–165. [PubMed: 11337275]

4. Jankowsky JL, et al. Mutant presenilins specifically elevate the levels of the 42 residue beta-amyloid peptide *in vivo*: evidence for augmentation of a 42-specific gamma secretase. Hum. Mol. Genet. 2004; 13:159–170. [PubMed: 14645205]

5. Kawai M, Kalaria RN, Harik SI, Perry G. The relationship of amyloid plaques to cerebral capillaries in Alzheimer's disease. Am. J. Pathol. 1990; 137:1435–1446. [PubMed: 2260630]

6. Kumar-Singh S, et al. Dense-core plaques in Tg2576 and PSAPP mouse models of Alzheimer's disease are centered on vessel walls. Am. J. Pathol. 2005; 167:527–543. [PubMed: 16049337]

7. Hsiao K, et al. Correlative memory deficits, Aβ elevation, and amyloid plaques in transgenic mice. Science. 1996; 274:99–102. [PubMed: 8810256]

8. Hyman BT, et al. Quantitative analysis of senile plaques in Alzheimer disease: observation of log-normal size distribution and molecular epidemiology of differences associated with apolipoprotein E genotype and trisomy 21 (Down syndrome). Proc. Natl Acad. Sci. USA. 1995; 92:3586–3590. [PubMed: 7724603]

9. Itagaki S, McGeer PL, Akiyama H, Zhu S, Selkoe D. Relationship of microglia and astrocytes to amyloid deposits of Alzheimer disease. J. Neuroimmunol. 1989; 24:173–182. [PubMed: 2808689]

10. Frautschy SA, et al. Microglial response to amyloid plaques in APPsw transgenic mice. Am. J. Pathol. 1998; 152:307–317. [PubMed: 9422548]

11. Combs CK, Karlo JC, Kao SC, Landreth GE. β-Amyloid stimulation of microglia and monocytes results in TNFα-dependent expression of inducible nitric oxide synthase and neuronal apoptosis. J. Neurosci. 2001; 21:1179–1188. [PubMed: 11160388]

12. Qin S, et al. System Xc- and apolipoprotein E expressed by microglia have opposite effects on the neurotoxicity of amyloid-β peptide 1–40. J. Neurosci. 2006; 26:3345–3356. [PubMed: 16554485]

13. Schenk D, et al. Immunization with amyloid-β attenuates Alzheimer-disease-like pathology in the PDAPP mouse. Nature. 1999; 400:173–177. [PubMed: 10408445]

14. Nagele RG, Wegiel J, Venkataraman V, Imaki H, Wang KC. Contribution of glial cells to the development of amyloid plaques in Alzheimer's disease. Neurobiol. Aging. 2004; 25:663–674. [PubMed: 15172746]

15. Simard AR, Soulet D, Gowing G, Julien JP, Rivest S. Bone marrow-derived microglia play a critical role in restricting senile plaque formation in Alzheimer's disease. Neuron. 2006; 49:489–502. [PubMed: 16476660]

16. Games D, et al. Alzheimer-type neuropathology in transgenic mice overexpressing V717F β-amyloid precursor protein. Nature. 1995; 373:523–527. [PubMed: 7845465]

17. Jung S, et al. Analysis of fractalkine receptor CX(3)CR1 function by targeted deletion and green fluorescent protein reporter gene insertion. Mol. Cell. Biol. 2000; 20:4106–4114. [PubMed: 10805752]

18. Bacskai BJ, et al. Imaging of amyloid-β deposits in brains of living mice permits direct observation of clearance of plaques with immunotherapy. Nature Med. 2001; 7:369–372. [PubMed: 11231639]

19. Geula C, et al. Aging renders the brain vulnerable to amyloid β-protein neurotoxicity. Nature Med. 1998; 4:827–831. [PubMed: 9662375]

20. Knowles RB, et al. Plaque-induced neurite abnormalities: implications for disruption of neural networks in Alzheimer's disease. Proc. Natl Acad. Sci. USA. 1999; 96:5274–5279. [PubMed: 10220456]

21. Le R, et al. Plaque-induced abnormalities in neurite geometry in transgenic models of Alzheimer disease: implications for neural system disruption. J. Neuropathol. Exp. Neurol. 2001; 60:753–758. [PubMed: 11487049]

22. Jarrett JT, Lansbury PT Jr. Seeding 'one-dimensional crystallization' of amyloid: a pathogenic mechanism in Alzheimer's disease and scrapie? Cell. 1993; 73:1055–1058. [PubMed: 8513491]

23. Meyer-Luehmann M, et al. Exogenous induction of cerebral β-amyloidogenesis is governed by agent and host. Science. 2006; 313:1781–1784. [PubMed: 16990547]

24. Walsh DM, et al. Naturally secreted oligomers of amyloid-β protein potently inhibit hippocampal long-term potentiation *in vivo*. Nature. 2002; 416:535–539. [PubMed: 11932745]

25. Lesne S, et al. A specific amyloid-β protein assembly in the brain impairs memory. Nature. 2006; 440:352–357. [PubMed: 16541076]

26. Spires TL, et al. Dendritic spine abnormalities in amyloid precursor protein transgenic mice demonstrated by gene transfer and intravital multiphoton microscopy. J. Neurosci. 2005; 25:7278–7287. [PubMed: 16079410]

27. Klunk WE, et al. Imaging Aβ plaques in living transgenic mice with multiphoton microscopy and methoxy-X04, a systemically administered Congo red derivative. J. Neuropathol. Exp. Neurol. 2002; 61:797–805. [PubMed: 12230326]
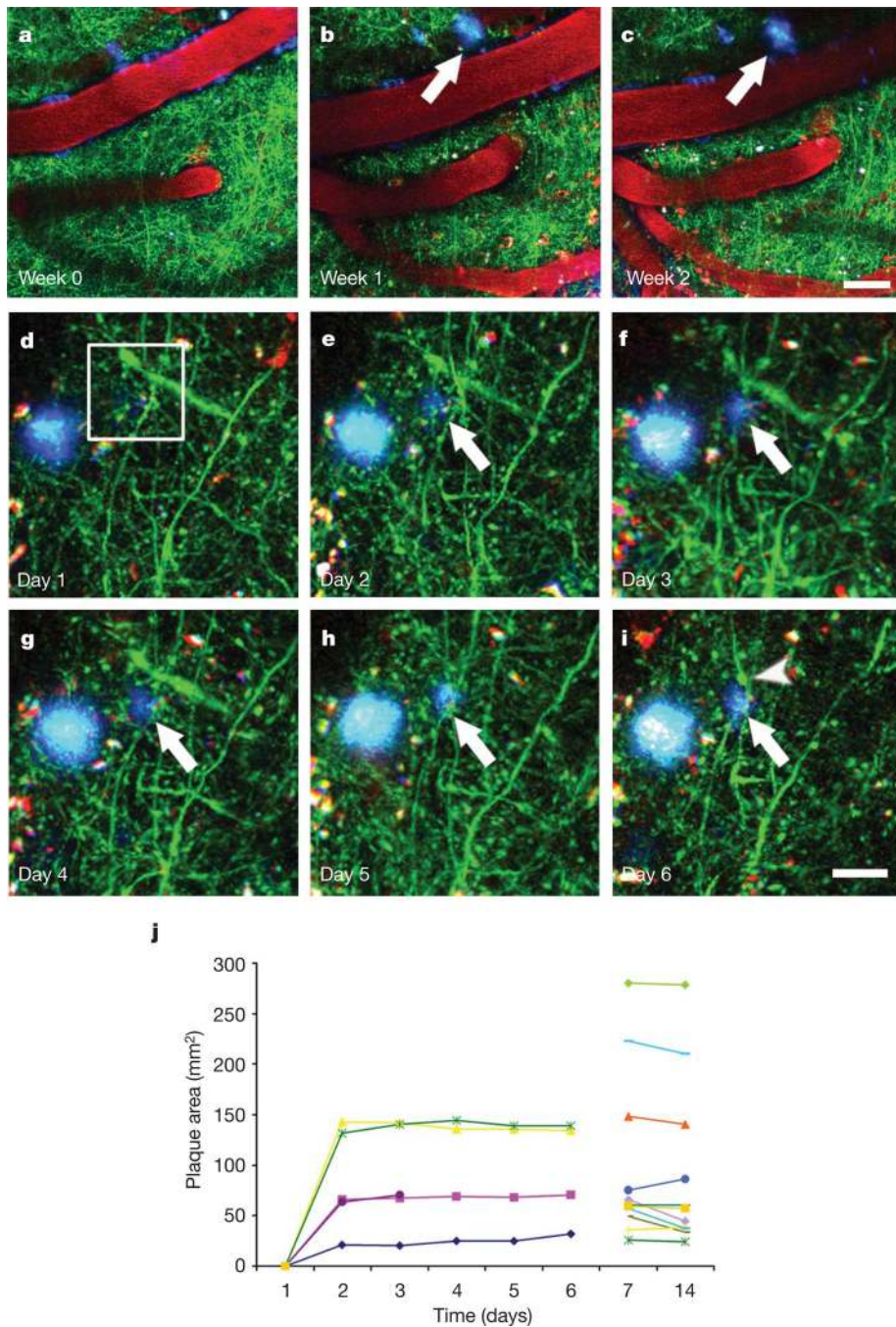
**Figure 1. Appearance of a novel plaque is a rapid process**

a–c, Low-magnification images provide an overview of the areas of potential plaque formation. The angiogram (red, Texas red), amyloid deposition (blue, methoxy-XO4) and neurons (green, YFP) are easily identified on the initial day of surgery (**a**) as well as one week (**b**) and two weeks later (**c**), allowing reimaging of the same sites over different imaging sessions. A new parenchymal amyloid deposition was identified one week (**b**) and two weeks (**c**) after the first imaging at this site. The new plaque appearing is indicated by an arrow (**b** and **c**). **d–i**, Sequential daily imaging of a potential plaque-formation area revealed that plaques can form rapidly in a short time interval from one day to another (**e**). The initial plaque was joined by a novel plaque marked with arrows over six consecutive

days (**e–i**). Note the formation of a dystrophy indicated by an arrowhead (**i**). A line diagram was used in this figure to visualize plaque size over time. The mean area of new plaques was 88.7 ± 69.3 µm^2 (mean ± s.d.) (n = 18). This is comparable to the mean plaque area of 93.7 ± 74.8 µm^2 (mean ± s.d.) (n = 153) (Student's t-test not significant, P = 0.77) measured post mortem in a subset of these animals by using the Bioquant image analysis system. Each individual plaque that appeared either after one day or seven days is represented by a different colour (**j**). Scale bars, 30 µm (**a–c**) and 20 µm (**d–i**).
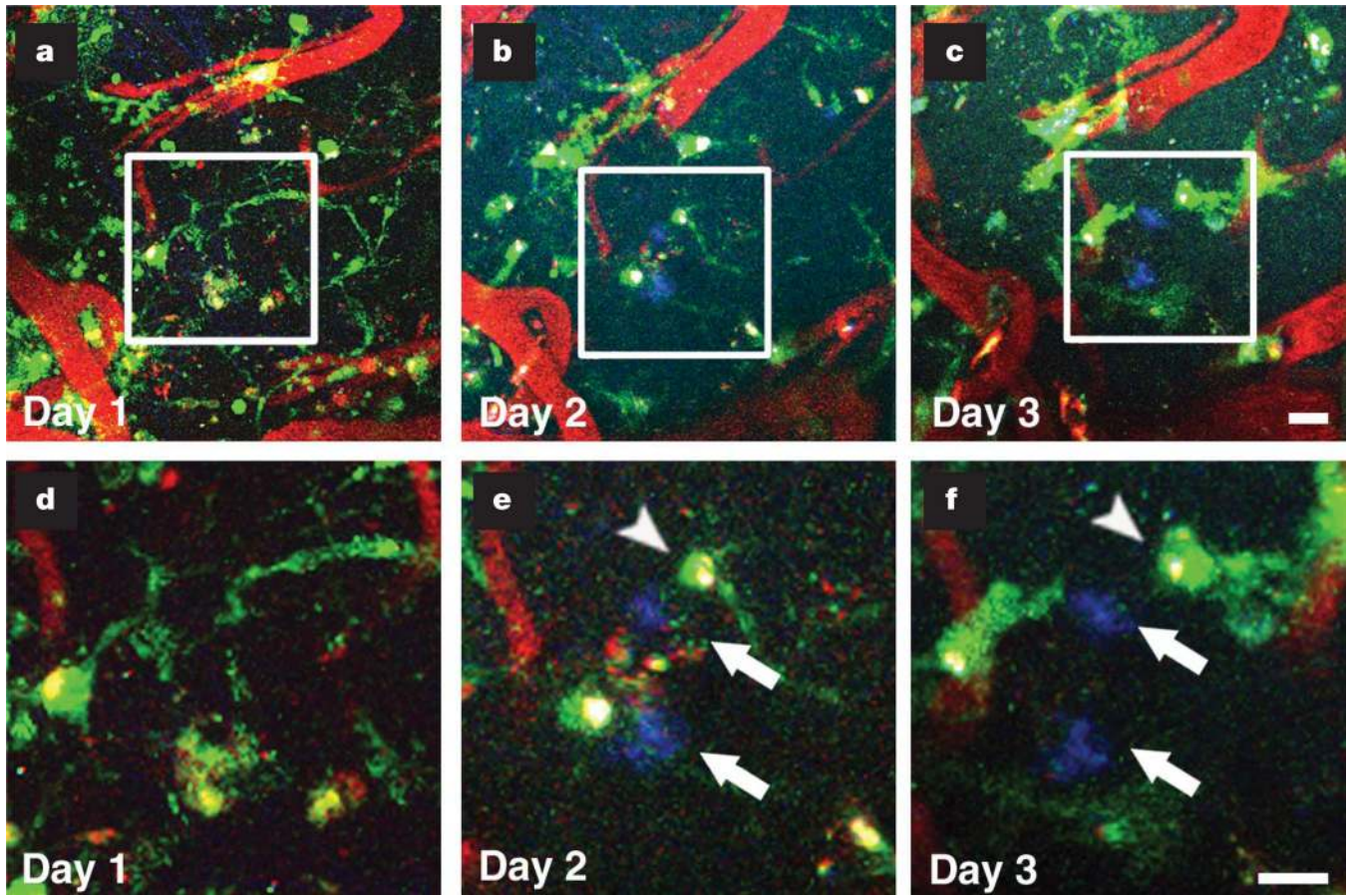
Figure 2. Microglia recruitment follows plaque formation
a–f, Green fluorescent protein-positive microglia cells were imaged in
PDAPP$^{+/-}$CX3CR1$^{+/-}$ mice before and after plaque formation in daily imaging sessions. **b**,
e, Two plaques appeared within 24 h (arrows) as well as microglia around these newly
formed plaques. Individual microglia remained stable but new microglia surrounding
plaques were also evident (arrowhead). Scale bars, 20 µm.
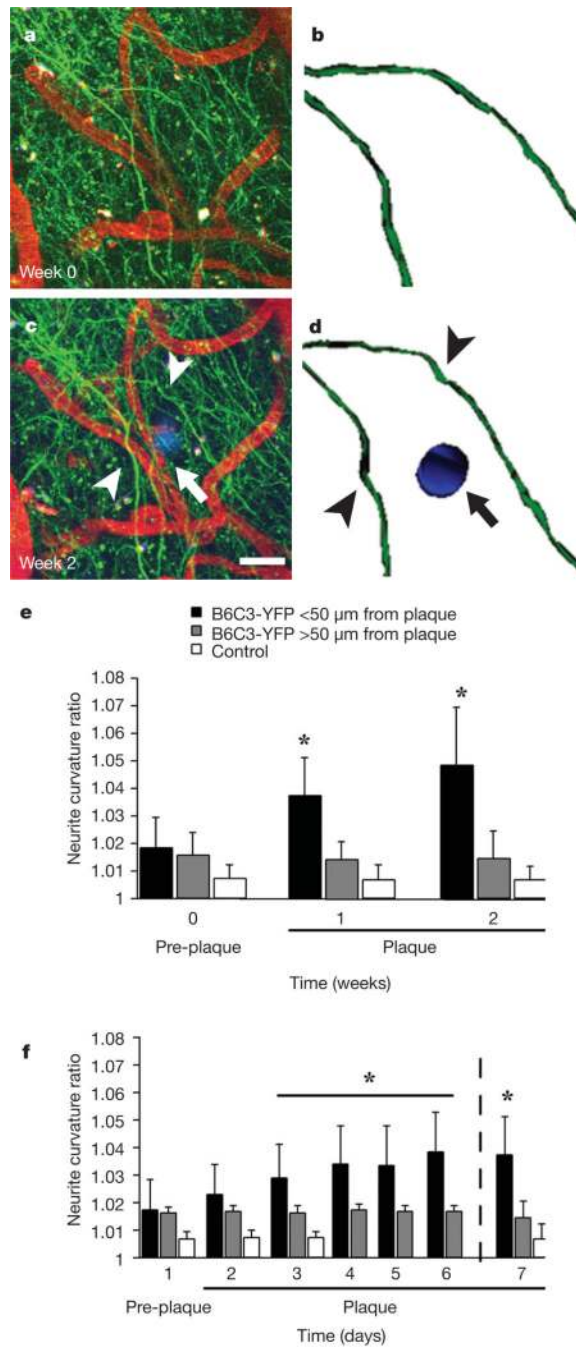
Figure 3. Plaque formation has no immediate effect on neuritic curvature
a–d, Neurites were observed before and after plaque formation. A new plaque labelled with methoxy-XO4 is shown in **c** and indicated by an arrow. Images from the green channel were further analysed and neurite curvature was measured. Arrowheads in **c** and **d** denote the increased neurite curvature after a plaque formed. Three-dimensional reconstruction as an example of a developed plaque (blue) surrounded by deforming neurites (green) (**b**, **d**). Scale bar, 50 µm. **e**, Neurite curvature was measured one week before and after plaque development. Neurites ($n = 29$) measured in B6C3-YFP mice ($n = 6$) less than 50 µm from a plaque, neurites more than 50 µm from a plaque ($n = 27$) and neurites ($n = 40$) in control mice ($n = 5$) are depicted as black, grey and white bars, respectively. There was a

statistically significant increase in neurite curvature after plaques form compared with the initial imaging session one week earlier. This increase persists one week after formation (two weeks from initial time point) (asterisk, ANOVA $P < 0.0001$). **f**, Daily assessment of neurite curvature changes ($n = 12$) from five new plaques revealed no significant differences at the day of plaque occurrence (data from all new plaques normalized to show plaque appearance at day 2). However, there was a tendency towards increased curvature, which became statistically significant at the third imaging day, one day after plaque appearance (asterisk, ANOVA $P = 0.002$). At imaging day 6, the neurite curvature ratio reached the highest level (asterisk, ANOVA $P = 0.0002$) and was comparable to that seen one week after plaque formation (day 7). Data are shown as mean ± standard deviation.